Few-body quantum dynamics of high-*Z* ions studied at the future relativistic high-energy storage ring

S Hagmann[1,2], **Th Stöhlker**[2,3,4], **Yu Litvinov**[2], **C Kozhuharov**[2],
P-M Hillenbrand[2,5], **U Spillmann**[2], **V Shabaev**[2,6], **K Stiebing**[1],
M Lestinsky[2], **A Surzhykov**[7], **A Voitkiv**[8], **B Franzke**[2], **D Fischer**[7],
D Schneider[9,10], **D Jakubassa**[11], **A Artiomov**[12], **E DeFilippo**[13], **X Ma**[14],
R Dörner[1] **and H Rothard**[15]

[1] Institut für Kernphysik, Universität Frankfurt, Frankfurt, Germany
[2] GSI-Helmholtzzentrum, Darmstadt, Germany
[3] Physik Institut, Universität Jena, Jena, Germany
[4] Helmholtz-Institut, Jena, Jena, Germany
[5] Institut für Atom- und Molekülphysik, Universität Giessen, Germany
[6] Department of Physics, State University, Saint Petersburg, Russia
[7] Physik Institut Universität Heidelberg, Heidelberg, Germany
[8] Max Planck Institut für Kernphysik, Heidelberg, Germany
[9] Extreme Matter Institute EMMI, Darmstadt, Germany
[10] LLNL, Livermore, USA
[11] Mathematics Institute LMU-München, Germany
[12] Veksler and Baldin Laboratory, JINR, Dubna, Russia
[13] INFN-LNS Sezione di Catania, Catania, Italy
[14] Institute of Modern Physics, Lanzhou, People's Republic of China
[15] CIRIL-GANIL, Caen, France

E-mail: s.hagmann@gsi.de

Abstract
At the FAIR facility for antiprotons and ion research, the high-energy storage ring will provide
highly charged heavy ions with *Z* all the way to $Z = 92$ for beam energies ranging from
200 A MeV up to energies of approximately 5 A GeV. This opens up a wealth of opportunities
for in-ring atomic physics experiments on few-body quantum dynamics ranging from, for
example, the correlated dynamics of various e^+–e^- pair creation processes to
quasi-photoionization of inner shells of the highest-*Z* ions.

PACS numbers: 34.50.−s, Rk, 34.70+e, 34.80.−i, 29.20.Dh, 29.30.−h, 25.75.−q, 41.60.−m

(Some figures may appear in colour only in the online journal)

1. Introduction

Heavy-ion storage rings—such as ESR and TSR (www.gsi.de/gsiwork/beschleuniger/esr.htm and www.mpi-hd.mpg.de/blaum/storage-rings/tsr/index.en.html)—have for many years furnished distinctive and singularly powerful instrumentation by providing highly luminous beams and extremely clean conditions for fundamental experiments in atomic spectroscopy and collision dynamics. In the following, we illustrate new opportunities for atomic physics in the relativistic domain opened by relativistic heavy ions in the new storage ring (high-energy storage ring (HESR)). This ring was originally conceived for experiments using antiprotons, but will also be made available for highly charged heavy ions by the FAIR project at GSI [1]. The future HESR storage ring with a maximal magnetic rigidity of $B\rho = 50$ T m
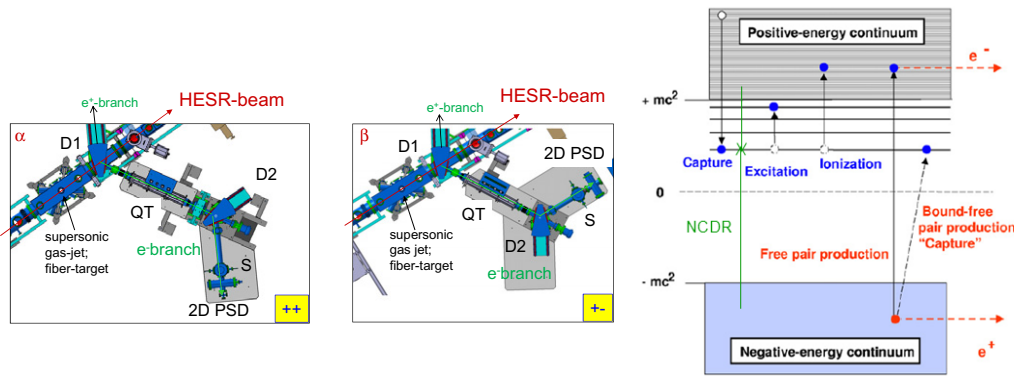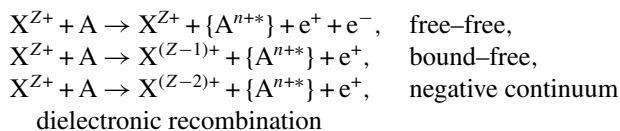
Figure 1. Left: two possible configurations for a forward imaging electron/positron spectrometer, corresponding to solid angle or momentum resolution optimization. Right: a schematic diagram of various electron excitation and pair creation processes in ion–atom collisions.

will be storing beams of heavy ions up to $Z = 92$ and with charge states up to bare ions for energies ranging from 200 to 5000 A MeV ($\gamma = 6$) and will thus provide a much welcomed extension into the relativistic region beyond the ESR. In the following, we give brief descriptions of selected experiments at this new storage ring and will mainly focus on experiments on few-body quantum dynamics of high-Z ions.

2. Electromagnetic e$^+$–e$^-$ pair production

In relativistic ion–atom collisions, it is most productive to interpret the observed electron–positron pair creation as a collision-induced transition from the negative continuum into the positive continuum [2–4] (for possible spectrometer configurations also permitting simultaneous and coincident detection of forward-emitted e$^+$ and e$^-$, see figure 1 (left)). Going along with experimental findings, one distinguishes 'free–free' transitions, where both electron and positron find themselves in a positive continuum state, from 'bound–free' transitions, where the electron is placed into a (final) bound state of the projectile. Whereas quasi-photoionization focuses on the regime of very small momentum transfers, collisions leading to electron–positron pair creation are characterized by very large momentum transfers: in these collisions a very different region of the electronic wavefunction is sampled. Experimental coincident angular and energy distributions of emitted positrons and electrons are needed by theory as benchmarks for most sensitive tests of the features of various theoretical models; in particular, for the heaviest collision partners between Au and uranium, the transient electromagnetic fields prohibit a theoretical treatment in first-order perturbation theory, as the observed ionization cross sections have to be ascribed in theory to multiphoton channels (see figure 1).

It is reasonable to formally distinguish three cases of electron–positron pair creation [2–4]:

$X^{Z+} + A \rightarrow X^{Z+} + \{A^{n+*}\} + e^+ + e^-$, free–free,
$X^{Z+} + A \rightarrow X^{(Z-1)+} + \{A^{n+*}\} + e^+$, bound–free,
$X^{Z+} + A \rightarrow X^{(Z-2)+} + \{A^{n+*}\} + e^+$, negative continuum
  dielectronic recombination

(with cross sections 3 b, 2 b and 42 μb at 1 A GeV U^{92+} [2, 4]; the shorthand $\{A^{n+*}\}$ indicates that during the high momentum

transfer pair creation simultaneously additional multiple outer shell ionization of the target atom A with production of one or more very low energy electrons is likely to occur; for simplicity all electrons that are spectators to the pair creation are omitted in the above reaction balances).

The collision energy dependence of the third channel exhibiting a maximum is very different from the collision energy dependence of the first two channels. For both, a monotonic increase of the cross section, $\sim(\ln)^3\gamma$ for 'free–free' and $\sim \ln \gamma$ for 'bound–free' pair creation, was predicted [2, 4, 5]. Only the distinct DCS for positrons (and electrons) gives access to the underlying dynamics.

3. 1s 'photo'-ionization of U^{91+} for $q \rightarrow 0$ momentum transfer and eV-'photo'-electron energy resolution

For the ionization of atoms or ions in the relativistic regime via photons or charged particles (such as electrons or highly charged ions), it is highly instructive to compare the resulting emission characteristics of emitted electrons. The reason is revealed when one considers the theoretical treatment of these processes, which takes advantage of the fact that particularly in very fast collisions at large impact parameters the electromagnetic field of a relativistic and charged projectile resembles the one created by a photon pulse; this equivalence is not given in slow collisions. For low-Z ions or atoms, this analogy of the impact ionization in the dipole limit (i.e. in the nonrelativistic Bethe–Born approximation) with ionization resulting from photoabsorption emerges in total ionization cross sections and can even be traced to the parameters of the angular distribution of the 'quasi-photo-electrons'; this has been successfully exploited in molecular spectroscopy [5]. For low-Z ions, a state-of-the-art theoretical calculation [5] for ionization cross sections and angular distributions for low-energy electron impact is compared for $\gamma = 2$ and 100 in figure 2 (left).

The middle and right diagrams in figure 2 illustrate eV electron energy resolution in the emitter frame and that fast and slow electrons in an ionizing collision at relativistic energies may appear in the laboratory at energies and observation angles convenient for current spectrometers. However, it has been pointed out in many treatises on relativistic collisions that the situation is far more complex
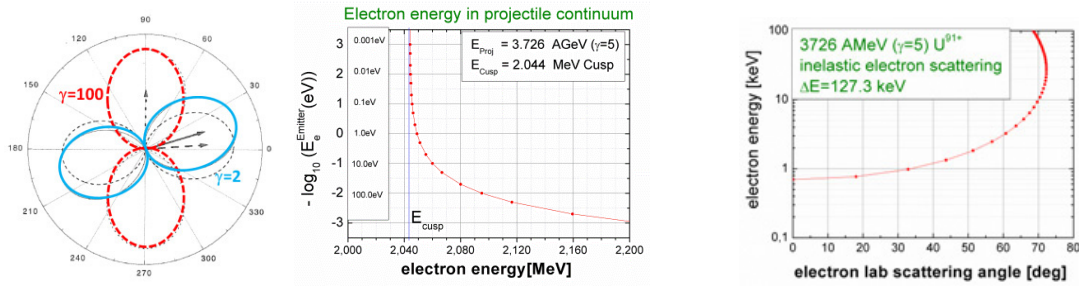
Figure 2. Left: theoretical angular distribution of electrons from p + H collisions for $q_{\text{perpendicular}} \times 10^{-3}$ au; note rotation of the pattern for high γ [5]. Middle and right: electron energies for fast and slow electrons for (*e*, 2*e*) collisions.

for $|k_b| = |K|$ there is a unique relation between Θ_b and p
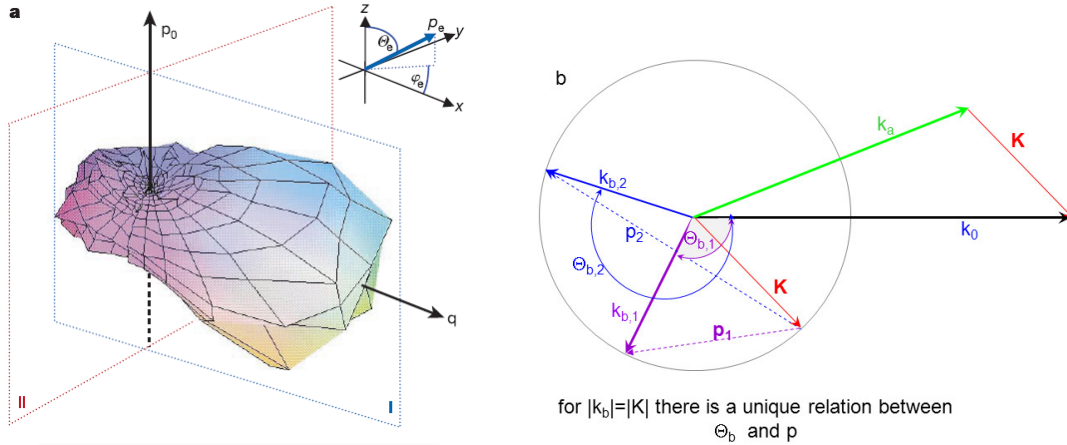
Figure 3. Left: complete differential cross section for single ionization in 100 A MeV C^{6+} + He collisions [6]. Right: kinematics for (*e*, 2*e*) collisions close to the Bethe ridge condition.

in the relativistic regime for high-Z ions/atoms and for electrons in innermost orbitals [5]. The HESR offers unique experimental conditions for differential ionization cross sections at relativistic velocities and for high Z in order to explore this regime, which is of utmost interest for advanced *ab initio* theories in the 'optical limit' where in the limit the momentum transfer $k \to 0$. Kinematic calculations for $\gamma = 5$ collisions for $U^{91+}(1s) + He \to U^{92+} + e_{\text{fast}}(0^0, \text{Cusp}) + e_{\text{slow}}(\theta_{\text{slow}})$ for $q \to 0$ show that in the laboratory frame the corresponding electrons can be well analysed by using a combination of a reaction microscope and an imaging forward electron spectrometer (see figure 2 (middle)). Relevant data for detailed comparisons with relativistic photoionization will then be produced in pertinent storage ring experiments.

4. Relativistic and QED effects in momentum density profiles $|\psi(1s)|^2$ via (*e*, 2*e*) spectroscopy in very heavy ions and in inverse kinematics: momentum profile in $U^{91+}(1s) + He \to U^{92+} + e_a(\theta_a) + e_b(\theta_b)$

The HESR, which can store the heaviest H-like and He-like ions, offers distinct advantages for in-ring experiments in inverse kinematics when one considers ionizing collisions in the coplanar asymmetric configuration (see figure 3(a)); this configuration will cover most of the ionization cross section, but can also be used at sufficiently high collision velocities to map the state-resolved initial-state momentum profile of the ionized electrons very efficiently. As is illustrated

in figure 3, the initial state momentum profile imaging in coplanar asymmetric configuration requires that for one angle θ_b the Bethe ridge condition $\mathbf{k_b} = \mathbf{K}$ be fulfilled [7], i.e. negligible momentum transfer to the recoiling ion during the collision (see equation (1)):

$$A^{(z-1)+}(1s) + He \to A^{z+} + e_a(\theta_a) + e_b(\theta_b) + \{He^{+^*}\}. \quad (1)$$

θ_a and θ_b correspond to laboratory detection angles, and the He atom here serves as a target of quasi-free electrons. Electrons e_b, when ionized out of the projectile, will be produced mostly with a low kinetic energy in the continuum of the projectile and will thus appear in the laboratory at small angles θ_b with respect to the projectile direction; this makes momentum analysis of these electrons using an imaging forward electron spectrometer most attractive due to it nearly covering 4π in the emitter frame. The ionizing electron e_a appears in the final state of the collision in the laboratory system with a low kinetic energy (as this corresponds to an inelastic collision with moderate energy loss in the projectile frame) and can be momentum analysed efficiently with a reaction microscope in coincidence with the swift forward electron. The momentum diagram of figure 3 shows how the relationship between measured coincident angular distributions of the ionized electron, i.e. the differential ionization cross section, and the initial-state one-electron momentum density profile may be established. In Betheridge kinematics, the ionized electron has an emitter frame momentum $|k_b| = |K|$. In the scattering plane, the
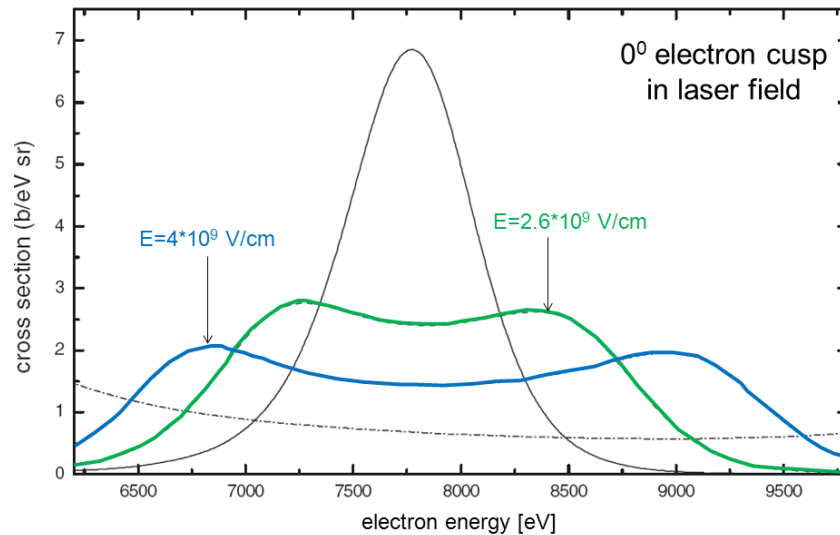
Figure 4. $0°$-electron cusp for 3.6 A MeV He$^+$ + H collisions [8]; without a field (full line) and in the presence of a CO$_2$ laser field ($\lambda = 10.6\,\mu$m) of two different field strengths.

vector k_b thus describes a circle around a foot point of k_0 (of a sphere if one wants to also consider scattering outside the plane). In binary collisions, one has the vector relation $k_b - p = K$ for every emission angle θ_b; it follows that each angle θ_b is attributed to a well-defined initial-state momentum p of the electron. This means that the probability measured for an electron at angle θ_b is proportional to the probability of an electron in the initial state to have momentum p; the triply differential ionization cross section is thus proportional to the one-electron momentum density $|\psi(p)|^2$. This opens a sensitive technique to identify for the first time momentum-dependent relativistic and QED contributions in the momentum profile.

5. Laser-assisted ion–atom collisions: modification of electron emission

The advance of femtosecond (fs) and attosecond (as) high-power lasers and their interaction with atoms and molecules has significantly expanded our understanding of the dynamics of field-assisted electron–ion interaction in the time domain of atomic electronic transitions down to 10^{-18} s. All these observations resulted from now well-established 2-colour fs/as spectroscopy of atoms and molecules. Another promising approach is investigating electron–ion collisions in a superimposed laser field, as has been successfully demonstrated in laser-induced recombination at the ESR [9]. Similarly, Voitkiv [8] predicts a remarkable effect in the $0°$

binary encounter, i.e. the elastic backscattering of a target electron in the projectile potential, where the prominent single peak splits in an IR field, the splitting given by $\Delta E = \bar{E} * \frac{p_s}{\omega_s}$ in the nonrelativistic domain (see figure 4). Here for relativistic collisions the binary encounter energy at $0°$ follows in simple two-body kinematics to be $\gamma_{BE} = 2\gamma^2 - 1$, where γ characterizes the projectile energy. This predicts extreme effects at the HESR already for moderate laser fields.

References

[1] Stoehlker T *et al* 2012 SPARC@HESR, a feasibility study, GSI 2012 (available at https://www.gsi.de/fileadmin/ SPARC/documents/SPARC@HESR_FS_V26.pdf)
    Stoehlker T *et al* 2013 *Phys. Scr.* **T156** 014085
[2] Artemyev A *et al* 2009 *Phys. Rev.* A **79** 032713
[3] Baltz A *et al* 2008 *Phys. Rep.* **458** 1
[4] Belkacem A *et al* 1997 *Phys. Rev.* A **56** 2806
[5] Voitkiv A and Ullrich J 2008 *Relativistic Collisions* (*Springer Series AOPP* vol 49) (Berlin: Springer)
[6] Schulz M *et al* 2003 *Nature* **422** 48
[7] Lahmam-Bennani A *et al* 1991 *J. Phys B: At. Mol. Opt. Phys.* **24** 2401
[8] Voitkiv A *et al* 2001 *J. Phys B: At. Mol. Opt. Phys.* **34** 4383
[9] Borneis S *et al* 1994 *AIP Conf. Proc.* **329** 150
    Borneis S *et al* 1994 *Phys. Rev. Lett.* **72** 207